1 Supplementary Information

Valence band photoelectron spectra

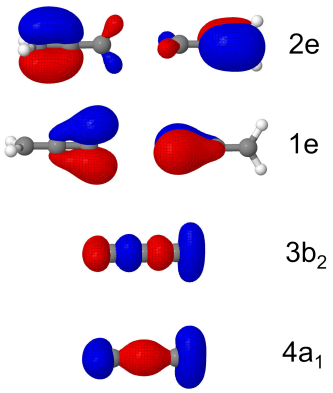

Fig. 1 Symmetry-adapted canonical valence molecular orbitals calculated at the EOM-CCSD/cc-pVTZ level.

Table 1 Total photoionisation cross sections in a.u. for the incident photon energy of 65 eV at the EOM-IP-CCSD/cc-pVTZ level for the minimum energy structure using ezDyson v5.0 code. [1,2]

orbital	Coulomb wave	plane wave
2e	0.040	0.155
1e	0.073	0.250
$3b_2$	0.211	0.465
$4a_1$	0.045	0.149

Dyson norms can serve as a quick estimate of the ionization intensities in the valence band photoemission spectra. The norms of the EOM-CC right and left Dyson orbitals are not uniquely defined, we therefore used the approach defined in M. L. Vidal, A. I. Krylov and S. Coriani, Phys. Chem. Chem. Phys., 22 (2020) 2693-2703. We calculated the norms as a geometric average of right and left Dyson norms

$$||\phi^{\text{Dyson}}||^2 = ||\phi_L^{\text{Dyson}}|| \times ||\phi_R^{\text{Dyson}}||. \quad (1)$$

Table 2 Dyson orbitals norms at the EOM-IP-CCSD/cc-pVTZ for the minimum energy structure.

orbital	$\|\|\phi^{\text{Dyson}}\|\|^2$
2e	0.9481
1e	0.9333
$3b_2$	0.9433
$4a_1$	0.9282

X-ray photoelectron spectra

The ground state allene is a symmetric molecule ($\mathscr{D}_{2d}$ point group) with two non-equivalent carbon sites, the central carbon and terminal carbons. The ground state electronic structure is

$(1a_1)^2(1b_2)^2(2a_1)^2(3a_1)^2(2b_2)^2(4a_1)^2(3b_2)^2(1e)^4(2e)^4$.

The three first orbitals correspond to the core orbitals, the next three are inner-valence orbitals and the last five are valence band orbitals.

Benchmark calculations of vertical core-ionisation energies for MP2 optimized minimum energy structure of allene are provided in Table 3. CVS-EOM-IP-CCSD was employed with various basis sets to study the convergence with increasing basis set size. Fully uncontracted basis sets were also employed. As it is evident from the table, the convergence and accuracy of fully uncontracted basis sets is faster and better than for cc-pVXZ. However, the accuracy of the small cc-pVTZ basis set within the CVS-EOM-IP-CCSD approach is reasonable.

Table 3 Benchmark calculations of vertical core-ionisation energies in eV for allen optimized at the MP2/aug-cc-pVTZ level. Comb refers to a combined basis set cc-pVXZ on hydrogen atoms and cc-pCVXZ on carbon atoms, u- refers to fully uncontracted basis set

method	central carbon	terminal carbons
exp.	290.9	290.6
MOM/CCSD(T)/comb DZ	292.4	292.1
MOM/CCSD(T)/comb TZ	290.7	290.8
MOM/LC-ωPBE/comb DZ	291.1	290.8
MOM/LC-ωPBE/comb TZ	290.0	289.7
MOM/LC-ωPBE/comb QZ	290.0	289.6
CVS-EOM-IP-CCSD/cc-pVTZ	291.7	291.4
CVS-EOM-IP-CCSD/aug-cc-pVDZ	294.2	293.7
CVS-EOM-IP-CCSD/u-aug-cc-pVDZ	291.8	291.5
CVS-EOM-IP-CCSD/aug-cc-pVTZ	291.7	291.3
CVS-EOM-IP-CCSD/u-aug-cc-pVTZ	291.5	291.1
CVS-EOM-IP-CCSD/aug-cc-pVQZ	291.5	291.1
CVS-EOM-IP-CCSD/u-aug-cc-pVQZ	291.4	291.0
CVS-EOM-IP-CCSD/aug-cc-pCVDZ	293.0	292.5
CVS-EOM-IP-CCSD/u-aug-cc-pCVDZ	291.8	291.4
CVS-EOM-IP-CCSD/aug-cc-pCVTZ	291.5	291.1
CVS-EOM-IP-CCSD/u-aug-cc-pCVTZ	291.5	291.1

Table 4 Dyson orbitals norms at the fc-CVS-EOM-IP-CCSD/cc-pVTZ for the minimum energy structure.

orbital	$\|\|\phi^{\text{Dyson}}\|\|^2$
central carbon	0.8702
terminal carbons	0.8808

Table 5 Key geometrical parameters characterizing the optimized structure of allene in the ground and ionized states (ionisation of the 1s central carbon atom or 1s on the terminal carbon). The optimization was performed at the MOM/LC-ωPBE with either cc-pVDZ and cc-pCVDZ or cc-pVTZ and cc-pCVTZ basis sets

	C–C1	C–C2	C1–H1	C2–H2
MOM/LC-ωPBE/comb DZ				
ground state	1.3046	1.3046	1.0917	1.0917
1s central	1.2807	1.2807	1.0968	1.0968
1s terminal	1.2809	1.2858	1.0506	1.0957
MOM/LC-ωPBE/comb TZ				
ground state	1.2965	1.2965	1.0833	1.0833
1s central	1.2620	1.2620	1.0887	1.0887
1s terminal	1.2702	1.2726	1.0330	1.0875

Table 6 Upper table: Comparison of the calculated harmonic vibrational frequencies in cm^{-1} calculated at the MP2/aug-cc-pVTZ level for optimized allene with experimental values (fundamental frequencies).*A.G. Maki and R.A. Toth, J. Mol. Spectry, 17 (1965) 136 and I.M. Mills, W.L. Smith and J.L. Duncan, J. Mol. Spectry, 16 (1965) 349. Lower table: Comparison of the harmonic vibrational frequencies in cm^{-1} calculated at the LC-ωPBE/cc-pVTZ level in the ground electronic state and within the MOM approach at the same level of theory for core ionized states (ionization from the central or terminal carbon atoms). **The ionized states have lower symmetry,e.g. we do not use the respective irreducible representations for the vibrational modes (but the modes are ordered in the same way as in the upper table). The ground state vibrations with the E irreducible representation split to two vibrational modes in the ionized states

irred. rep.	vib. mode	MP2 ground	exp.*
A_1	ν_1	3159	3015
	ν_2	1493	1443
	ν_3	1089	1073
B_1	ν_4	913	865
B_2	ν_5	3161	3407
	ν_6	2014	1957
	ν_7	1446	1398
E	ν_8	3232	3486
	ν_9	1040	999
	ν_{10}	897	841
	ν_{11}	391	355

ground	ionized central C**	ionized terminal C**
3407	3250	3369
1468	1649	1357
1182	1363	1122
757	939	718
3762	3709	4135
2239	2444	2395
1364	1394	1639
3320	3129, 3295	3138, 3825
1089	985, 1222	1317, 1450
1000	873, 985	661, 690
394	328, 408	139, 431

X-ray absorption spectra

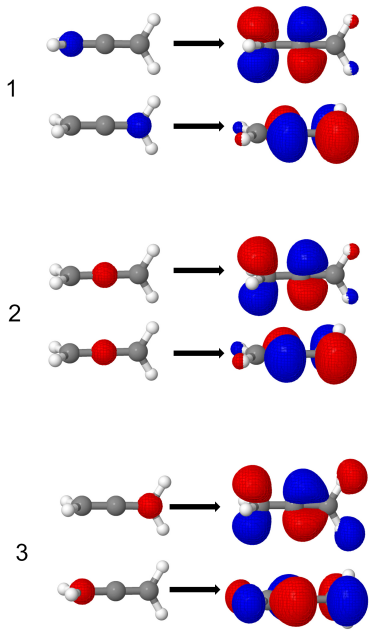

Fig. 2 Natural transition orbitals calculated at the CVS-EOM-EE-CCSD/cc-pVTZ level. Lowest-energy transition labeled as 1 corresponds to the two degenerate excitations from the core orbitals localized on the terminal carbons to the pair of unoccupied LUMO π^* orbitals. The two degenerate transitions corresponding to the excitations from the central carbon to the pair of LUMO π^* orbitals is labeled as 2. The two degenerate transition labeled as 3 again corresponds to excitation from the core orbitals localized on the terminal carbons to the pair of unoccupied LUMO π^* orbitals.

Table 7 Benchmark calculations of the core-excited states using CVS-EOM-EE-CCSD and TDDFT levels with various basis sets for the minimum energy structure. Lowest-energy transition labeled as 1 corresponds to the two degenerate excitations from the core orbitals localized on the terminal carbons to the pair of unoccupied LUMO π^* orbitals. The two degenerate transitions corresponding to the excitations from the central carbon to the pair of LUMO π^* orbitals is labeled as 2. The two degenerate transition labeled as 3 again corresponds to excitation from the core orbitals localized on the terminal carbons to the pair of unoccupied LUMO π^* orbitals.

method	1	2	3
TDDFT/LC-ωPBE/cc-pVDZ	270.27	270.70	271.37
TDDFT/LC-ωPBE/cc-pVTZ	269.83	270.30	270.90
CVS-EOM-IP-CCSD/cc-pVDZ	288.56	288.74	290.37
CVS-EOM-IP-CCSD/cc-pVTZ	285.88	286.07	287.64
CVS-EOM-IP-CCSD/aug-cc-pVDZ	288.34	288.59	289.96
CVS-EOM-IP-CCSD/u-aug-cc-pVDZ	286.07	286.20	287.69
CVS-EOM-IP-CCSD/aug-cc-pVTZ	285.80	285.95	287.46
CVS-EOM-IP-CCSD/u-aug-cc-pVTZ	285.53	285.68	287.20
CVS-EOM-IP-CCSD/aug-cc-pCVDZ	287.09	287.32	288.72
CVS-EOM-IP-CCSD/u-aug-cc-pCVDZ	286.04	286.18	287.66
CVS-EOM-IP-CCSD/aug-cc-pCVTZ	285.56	285.71	287.24
CVS-EOM-IP-CCSD/u-aug-cc-pCVTZ	285.50	285.64	287.18

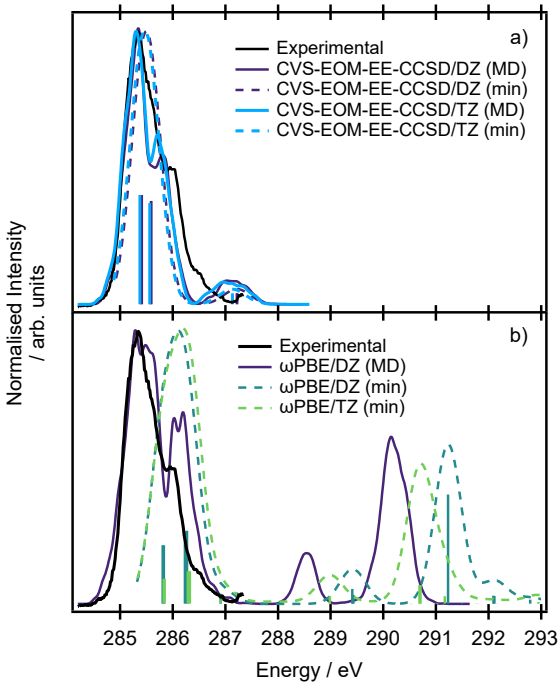

Fig. 3 XAS spectra for the minimum energy structure and within NEA at the CVS-EOM-EE-CCSD and TDDFT levels.The data for CVS-EOM-EE-CCSD/cc-pVDZ were shifted by 2.68 eV. The ωPBE/cc-pVDZ results were shifted by 15.55 eV and the ωPBE/cc-pVTZ were shifted by 16.0 eV.

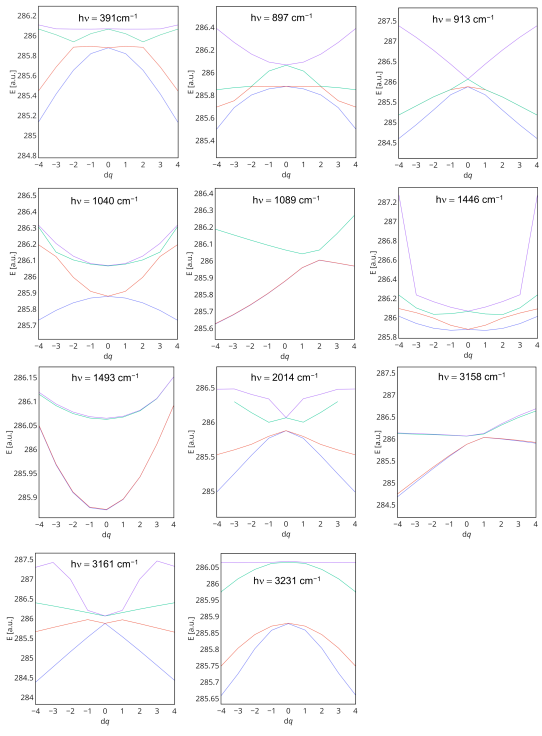

Fig. 4 Energy profiles calculated at the CVS-EE-CCSD/cc-pVTZ level for two degenerate lowest lying excited states (1 and 2 in Figure 2) in a. u. along all normal modes q_i (of the optimized ground state geometry). The dq values are given in units of a dimensionless normal-mode coordinate displacement.

Non-Condon effects in X-ray absorption spectra

The non-Condon effects describe the dependency of the transition dipole moment on the nuclear coordinate. The magnitude of the non-Condon effects can be evaluated from the comparison of the spectrum calculated within NEA with individiual transition dipole moments and a spectrum, which each geometry in NEA has the same transition dipole moment as the minimum energy structure. The spectra are presented in Fig. 5 and as can be seen, the shape and intensities of the spectral features are practically the same, e.g. the effect is only minor. The dependency of the transition dipole moment on vibrational coordinate is shown in Fig. 6. The particular molecular distorsions were constructed to correspond to variation of the normal coordinates from $-l_i\delta q_i$ to $-r_i\delta q_i$, where $-l_i$ and $-r_i$ specify the number of steps in positive and negative directions along each normal mode. As can be inferred from Fig. 6, the changes are not dramatic and do not manifest in the XAS spectra.

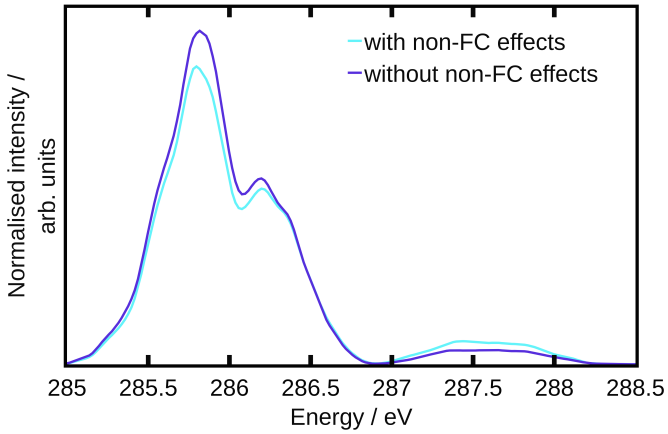

Fig. 5 XAS spectra simulated at the CVS-EOM-CCSD/cc-pVTZ level via NEA. The light blue line shows the full spectrum, e.g. for each geometry generated by MD an appropriate transition dipole moment was calculated. The violet line shows the spectrum in which we used the same value of the transition dipole moment corresponding to the minimum energy structure for all generated geometries.

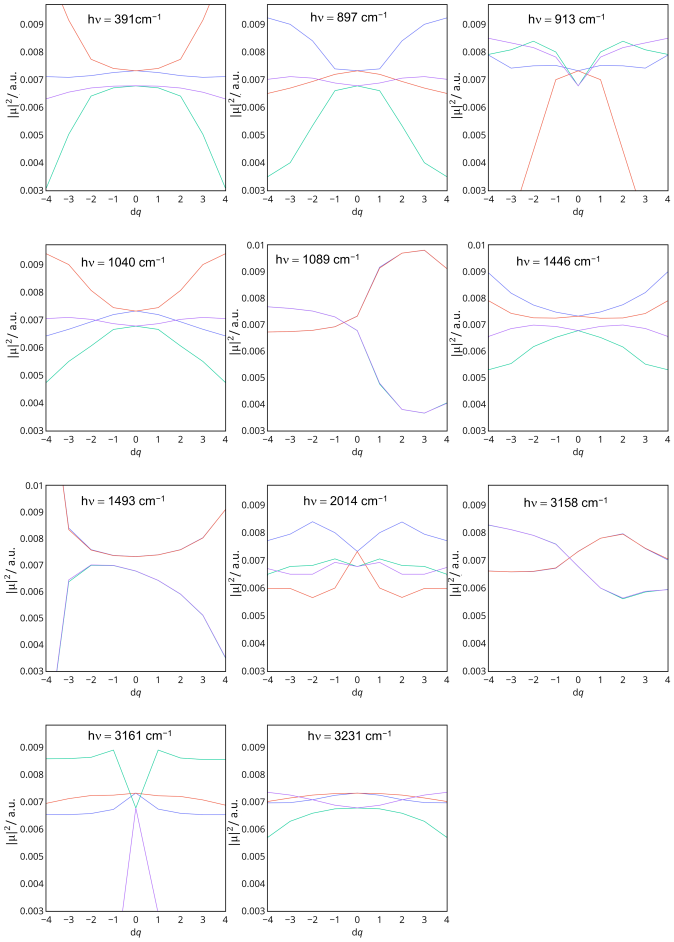

Fig. 6 Square of the transition dipole moment in a. u. along all normal modes q_i (of the optimized ground state geometry). The dq values are given in units of a dimensionless normal-mode coordinate displacement.

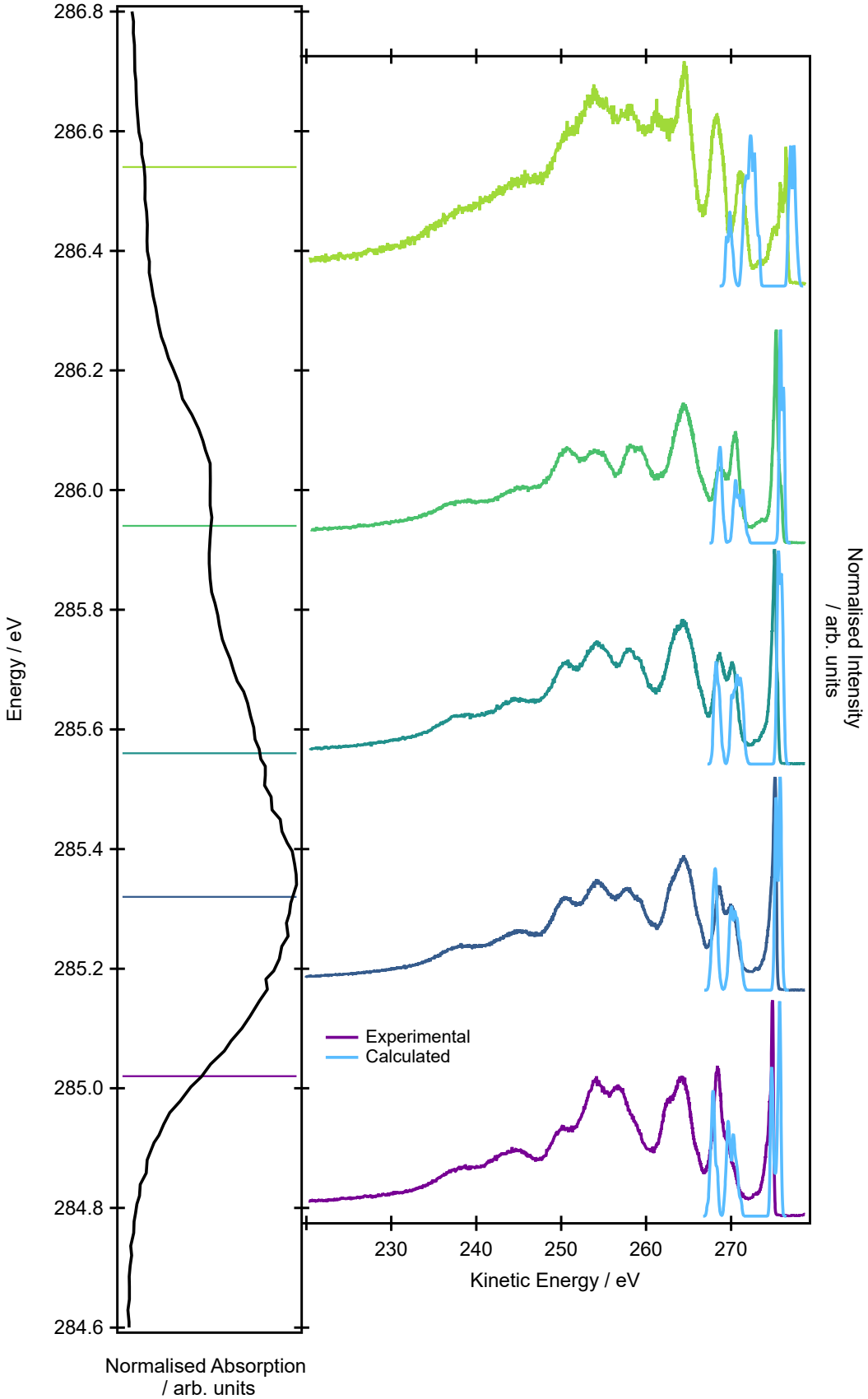

Fig. 7 Resonant Auger spectra. The left panel shows the XAS spectrum, the lines show energies at which the resonant Auger spectra were measured: 285.02, 285.32, 285.56, 285.94, 286.54 eV. The right panel shows individual resonant Auger spectra. The light blue line corresponds to the calculations at the EOM-CCSD/cc-pVTZ level for a set of structures with appropriate electronic transition energies (within 90 meV range).

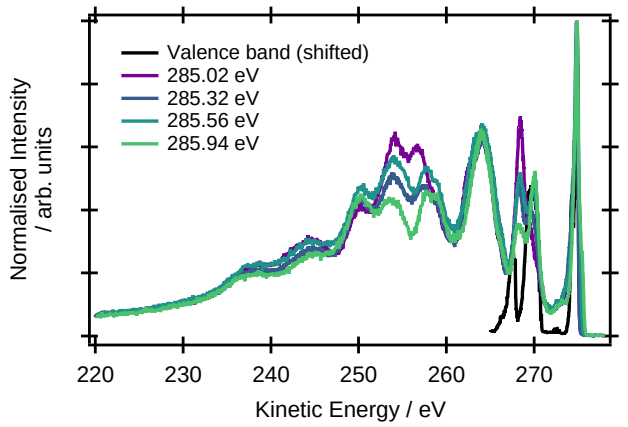

Fig. 8 Comparison of the resonant Auger spectra and shifted valence band spectrum

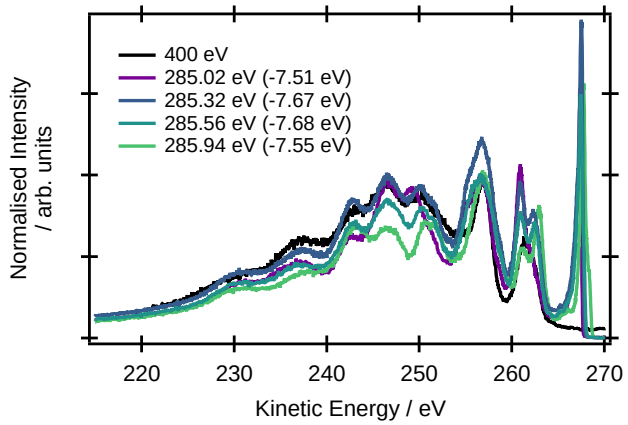

Fig. 9 Comparison of the resonant Auger spectra and the non-resonant Auger spectrum. The energies of the resonant Auger spectra have been shifted by the value in brackets in the figure label.

Notes and references

1 S. Gozem, A. O. Gunina, T. Ichino, D. L. Osborn, J. F. Stanton and A. I. Krylov, *Journal of Physical Chemistry Letters*, 2015, **6**, 4532–4540.

2 S. Gozem and A. I. Krylov, *The ezSpectra suite: An easy-to-use toolkit for spectroscopy modeling*, 2021, `http://iopenshell.usc.edu/downloads`.